

Microscopic origin of multiferroic order in monolayer NiI₂

Adolfo O. Fumega¹ and J. L. Lado¹

¹*Department of Applied Physics, Aalto University, 02150 Espoo, Finland*

The discovery of multiferroic behavior in monolayer NiI₂ provides a new symmetry-broken state in van der Waals monolayers, featuring the simultaneous emergence of helimagnetic order and ferroelectric order at a critical temperature of $T = 21$ K. However, the microscopic origin of multiferroic order in NiI₂ monolayer has not been established, and in particular, the role of non-collinear magnetism and spin-orbit coupling in this compound remains an open problem. Here we reveal the origin of the two-dimensional multiferroicity in NiI₂ using first-principles electronic structure methods. We show that the helimagnetic state appears as a consequence of the long-range magnetic exchange interactions, featuring sizable magnetic moments in the iodine atoms. We demonstrate that the electronic density reconstruction accounting for the ferroelectric order emerges from the interplay of non-collinear magnetism and spin-orbit coupling. We demonstrate that the ferroelectric order is controlled by the iodine spin-orbit coupling, and leads to an associated electronically-driven distortion in the lattice. Our results establish the microscopic origin of the multiferroic behavior in monolayer NiI₂, putting forward the coexistence of helical magnetic order and ligand spin-orbit coupling as driving forces for multiferroic behavior in two-dimensional materials.

I. INTRODUCTION

The emergence of symmetry-broken states in two-dimensional materials provides a unique opportunity for designing new forms of quantum matter in van der Waals heterostructures¹. Well known examples are van der Waals monolayers hosting superconducting^{2,3}, magnetic⁴⁻⁸, and ferroelectric^{9,10} orders. Interestingly, materials hosting two-different types of symmetry broken states allow for non-trivial couplings between different order parameters. Multiferroics¹¹⁻¹³ are a paradigmatic example of multiple symmetry breaking, where a material hosts simultaneous ferroelectric and magnetic orders. Two-dimensional multiferroics would provide disruptive possibilities for controlling magnetic order electrically^{14,15}, and to design electrically switchable magnetic van der Waals heterostructures¹⁶⁻²³. In the pursuit of 2D multiferroic orders, a variety of families of two-dimensional materials provide potential candidate materials^{16,24,25}. However, two-dimensional multiferroics have proven to be elusive.

Recent breakthrough experiments have shown the emergence of multiferroic symmetry-breaking in ultrathin NiI₂, leading to van der Waals materials displaying simultaneous magnetic and ferroelectric order. In particular, multiferroic behavior down to the bilayer,²⁶ and ultimately to the monolayer limit²⁷ was observed in NiI₂. The monolayer of NiI₂ shows a magnetic transition temperature $T = 21$ of K²⁷, and at the very same temperature, a finite ferroelectric polarization emerges. In bulk compounds, a variety of mechanisms are known to drive multiferroic behavior²⁸⁻³⁰, yet the origin of multiferroicity in monolayer NiI₂ remains an open question.

Here we address the microscopic origin of multiferroicity in NiI₂ using first-principles methods. In particular, we show that the combination of a helical magnetic state together with the strong spin-orbit coupling of iodine leads to the emergence of a finite electric dipole. Our results highlight the existence of a multiferroic state with

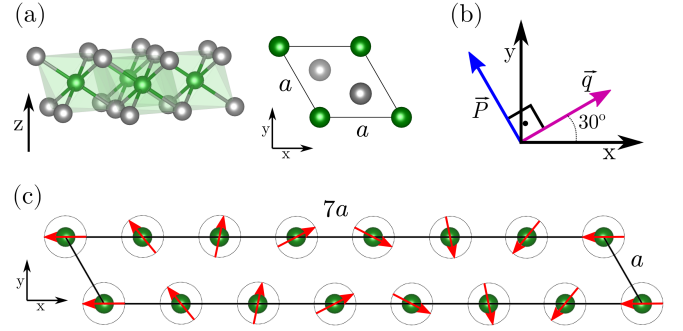


FIG. 1. (a) Structure of monolayer NiI₂, showing top and side views. Ni atoms are depicted in green and I in gray. (b) Propagation direction in real space of the spin-spiral vector (pink) of the helimagnetic order and the induced ferroelectric polarization (blue). (c) Representation of the helimagnetic order, showing a periodicity of 7×1 unit cells.

a strong magnetoelectric coupling in the monolayer limit of NiI₂, and establish its origin in the combination of the non-collinear magnetic state and spin-orbit coupling.

II. COMPUTATIONAL METHODS

We have performed *ab initio* electronic structure calculations based on density functional theory³¹ in NiI₂. Calculations were carried out with the all-electron full potential linearized augmented-plane-wave method, using a fully non-collinear formalism with spin-orbit coupling (SOC) as implemented in Elk³². We have used the local density approximation (LDA) for the exchange-correlation functional³³. The results presented are converged with respect to all the parameters, $2 \times 14 \times 1$ k-mesh and a vacuum spacing of 20 Å. Calculations of states with different helical states require careful convergence of the total electron density: with a 420×60 real space mesh for the electronic density and a convergence of

the Kohn-Sham potential of 10^{-7} a.u.. Moreover, to see the effect of the SOC in the formation of the spontaneous electric polarization, we have performed calculations scaling both the overall strength of the SOC interaction and the individual contribution of each atom by a dimensionless constant λ_{SOC} , where $\lambda_{\text{SOC}} = 1$ corresponds to the realistic limit.

III. HELIMAGNETIC STATE IN THE MONOLAYER

As a two-dimensional material, monolayer NiI_2 stems from a bulk van der Waals layered material. In its bulk form, NiI_2 is formed by van der Waals layers in the 1T phase, like the one shown in Fig. 1a. Neutron diffraction has confirmed that this compound undergoes a first magnetic transition at $T_{N,1} \sim 76$ K to an antiferromagnetic state with ferromagnetic (FM) planes. A second transition to a helimagnetic (HM) state that displays a finite electric polarization is observed at low temperatures ($T_{N,2} \sim 59.5$ K).^{34,35,36} Consequently, $T_{N,2}$ is not only the transition temperature to a HM, but to a multiferroic state in the bulk crystal. In the monolayer limit, the transition to the magnetically ordered states appears at $T_{N,2} = 21$ K, appearing at the same temperature a ferroelectric polarization. To unveil the origin of this multiferroic behavior, we start analyzing the magnetic order of monolayer NiI_2 .

In order to model the helimagnetic order in the monolayer, we approximate the incommensurate spin vector by the closest commensurate one $\mathbf{q} = \frac{1}{7}\mathbf{b}_1$.³⁷ The commensurate in-plane spin vector q -vector differs only by a $\sim 3.5\%$ from the incommensurate one. Therefore, the helimagnetic order is well captured in the monolayer with this spin arrangement. In real space, our approximate spin propagation vector \mathbf{q} is displayed along the [210] direction (in lattice vector units), thus perpendicular to the [010] direction as shown in Fig. 1b. Then, the helimagnetic order in the monolayer can be modeled with a $7a \times a$ supercell and an in-plane spin cycloid as shown in Fig. 1c.

We start addressing the electronic structure of the helimagnetic state. From a chemical point of view, NiI_2 shows a 1T-phase with Ni atoms in a Ni^{+2} state ($d^8 S=1$) in an octahedral iodine environment, leading to an effective $S = 1$ triangular lattice model developing the spin spiral state. As a reference, it is interesting to compare the results of the helimagnetic state with a hypothetical ferromagnetic one. The comparison between these magnetic configurations is performed without including SOC. The band structure plots for both configurations are shown in Fig. 2ab. A direct energy gap of ~ 200 meV coming from the $t_{2g} - e_g$ crystal field effect is found for both magnetic configurations. The existence of a gap in both configurations demonstrates that the insulating origin stems from strong electronic correlations, and not the spin spiral itself³⁸. A comparison between the highest

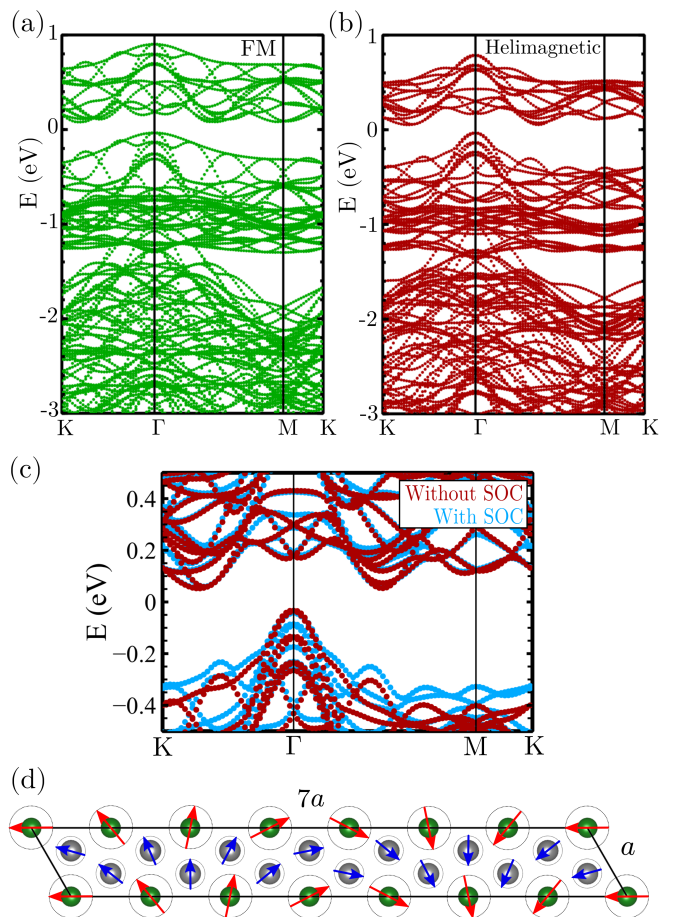


FIG. 2. Band structure plots for the ferromagnetic (a) and helimagnetic (b) states. A sizable energy gap can be seen for both configurations. (c) The effect of SOC in the helimagnetic state induces rearrangements in the band structure on the order of 50-100 meV. (d) Schematic of the magnetic polarization acquired by the I atoms in the helimagnetic state. Both the spin-vector direction and the helicity that occurs for the Ni atoms (red arrows) are transferred to the I atoms (blue arrows).

valence band of the helimagnetic and the FM configurations shows a decrease in the energies of the k-points for the HM. This is related to the energies found for each magnetic configuration.

The helimagnetic state is 27.7 meV per Ni atom lower in energy than the FM state. This result confirms that the helimagnetic state is, at least, a meta-stable low energy state at low temperature and, eventually, the ground state of 2D NiI_2 . It is interesting to note that, from a fully ionic picture, the system would be ferromagnetic according to the Anderson-Goodenough-Kanamori FM superexchange³⁹⁻⁴¹ mediated by the $\sim 90^\circ$ Ni-I-Ni bonds, in stark contrast with experiments and our first-principles calculations^{34,35}. The covalent nature of this compound introduces long-range exchange interactions that lead to the helimagnetic state³⁴. The compared energies of both configurations also show that the non-

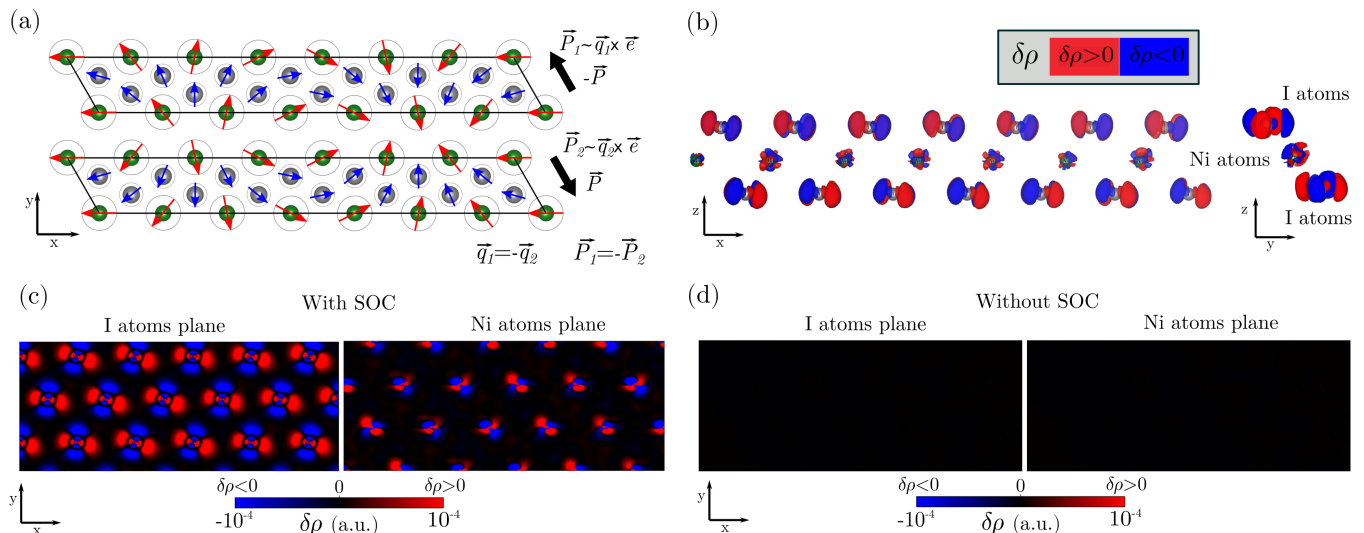


FIG. 3. (a) Schematic of the two different spin spiral configurations with opposite \mathbf{q} used to test the emergence of the electric dipole in the presence of SOC. (b) Three dimensional plots from different spatial perspectives of the electronic density difference $\delta\rho$ for the helimagnetic configurations with opposite helicity when SOC is included. This same quantity is shown as 2D plots in panels (c,d) for the planes of I and Ni atoms when the SOC is present (c) and absent (d). This unveils that an electronic reconstruction associated with the emergence of a spontaneous electric dipole is produced when SOC is introduced. It can be observed that the electronic rearrangement is larger around the I atoms than in the Ni ones. In the absence of spin-orbit coupling, both electronic densities are identical as shown in panel (d), signaling a zero electric polarization (fully black). These results show that the electronic reconstruction leading to a ferroelectric dipole stem from the combination of the helimagnetic state spin-orbit coupling.

collinear magnetic order in the 2D limit arises from the long-range magnetic isotropic exchange interactions and the lattice frustration. In particular, the relative sizes between first and long neighbor exchange determines the periodicity of the spin spiral order⁴². This is in agreement with previous analyses realized for the bulk³⁴. Therefore, our results highlight that the helimagnetic state does not rely on strong spin-orbit coupling effects^{43–45} as its driving force.

We now move on to consider the effect of spin-orbit coupling in the electronic structure of the helimagnetic state. First, it is interesting to compare the electronic dispersion in the absence and presence of SOC, as shown in Fig. 2c. In particular, it is clearly observed that states around the Fermi energy show variations on the order of 50-100 meV, well above the energy scale expected Ni spin-orbit coupling. This phenomenology alone suggests that the spin-orbit coupling effects of iodine can be the dominating factor for states close to the Fermi energy. It is worth noting that in order to obtain magnetic order at finite temperatures, spin-orbit coupling effects would provide the required SU(2) breaking terms in the Hamiltonian to overcome the Hohenberg-Mermin-Wagner theorem^{46–49}. The electronic reconstruction caused by the SOC will be related to the emergence of an electric dipole. Furthermore, our first-principles results reveal that for the helimagnetic configuration, the iodine atoms develop a sizable magnetization of $0.23 \mu_B$. Therefore, due to the covalency of this compound, I atoms are

substantially magnetized by the Ni atoms. Importantly, the helimagnetic state of the Ni atoms also occurs in the I atoms with the same spin propagation vector and helicity (see Fig. 2d). This effect will be crucial for the discussion of the emergence of a spontaneous electric polarization in the helimagnetic state.

IV. ORIGIN OF FERROELECTRIC ORDER

We now focus on analyzing the impact of spin-orbit coupling in the electronic structure, and in particular in the electronic density of the system. As the electronic density of the system determines the electric dipole, the mechanism for multiferroicity can be directly inferred from change in the electronic density. From a Ginzburg-Landau perspective and symmetry considerations^{28,50}, the existence of a helical state allows for the emergence of a ferroelectric dipole associated to the non-collinearity of the form

$$\mathbf{P} = \xi \mathbf{q} \times \mathbf{e} \quad (1)$$

where \mathbf{P} is the electric polarization, $\mathbf{e} = (0, 0, 1)$ the spin rotation axis and $\mathbf{q}_0 \approx \frac{1}{7} \mathbf{b}_1$ the \mathbf{q} -vector of the spin spiral, with \mathbf{b}_1 the reciprocal lattice vector of NiI_2 , and ξ is a scalar parameter that we will see that has a linear dependence with SOC and that has the same units as the electric polarization. In particular, Eq. (1) shows

that two spin spiral configurations with $\mathbf{q}_1 = \mathbf{q}_0$ and $\mathbf{q}_2 = -\mathbf{q}_0$ will give rise to opposite electric polarizations $\mathbf{P}_1 = -\mathbf{P}_2$ (Fig. 3a). The emergence of opposite electric dipoles can be directly observed in the total electronic density of the system. We perform first principles calculations in magnetic configuration with both \mathbf{q} -vectors, \mathbf{q}_1 and \mathbf{q}_2 (Fig. 3a). Both configurations are energetically equivalent, and therefore show same energies with and without spin-orbit coupling.

To reveal the emergence of the electric dipole, we now analyze the difference in the total electronic densities ρ_1 and ρ_2 , associated with ground states with \mathbf{q}_1 and \mathbf{q}_2 , respectively. In particular, the difference between these two electronic densities directly shows in real space the origin of the associated ferroelectric dipole, as the configurations will show opposite ferroelectric polarizations $\mathbf{P}_1 = -\mathbf{P}_2$. First, we show in Fig. 3b the electronic difference $\delta\rho = \rho_1 - \rho_2$ in real space between the two spin-spiral configurations with spin-orbit coupling. In particular, it is clearly observed that the changes in the density are maximal in the iodine atoms, highlighting the dominant role of iodine in the rearrangement of the electronic charge, ultimately leading to an electric dipole. The dominant role of iodine is also observed by showing the contribution of the iodine and Ni to the electronic reconstruction as shown in Fig. 3c, showing that the reconstruction is maximal in the iodine plane. Finally, we address the case without spin-orbit coupling, shown in Fig. 3d. In this case, it is clearly observed that the charge density is the same for both spin spirals, leading to a zero contribution to the electric dipole. The previous results highlight that the combination of helical order and spin-orbit coupling is responsible for the charge reconstruction leading to an electric dipole.

The previous discussion was focused on the electronic contribution to the electric polarization. Nevertheless, apart from this electronic contribution, the rearrangement of the electronic density will also have an impact on the lattice, leading to a small atomic relaxation associated with the ferroelectric electronic density. This lattice contribution can be directly imaged by comparing the small lattice relaxations associated with the helical orders \mathbf{q}_1 and \mathbf{q}_2 . In particular, we now characterized the ferroelectric atomic relaxation by the component in the forces associated with the two configurations with opposite ferroelectric vectors as

$$\mathcal{F}_\alpha = \frac{1}{2}(\mathbf{F}_\alpha[\mathbf{q}_1] - \mathbf{F}_\alpha[\mathbf{q}_2]) \quad (2)$$

where $\mathbf{F}_\alpha[\mathbf{q}_1]$, $\mathbf{F}_\alpha[\mathbf{q}_2]$ is the total force for atom α for the spin spiral state \mathbf{q}_1 , \mathbf{q}_2 respectively⁵¹. In the absence of spin-orbit coupling, the ferroelectric force \mathcal{F}_α is exactly zero, consistent with the vanishing difference in the electronic densities shown in Fig. 3d. In stark contrast, in the presence of the helical order and spin-orbit coupling, the emergent electronic reconstruction leads to opposite atomic relaxations for \mathbf{q}_1 and \mathbf{q}_2 , yielding a finite \mathcal{F}_α .

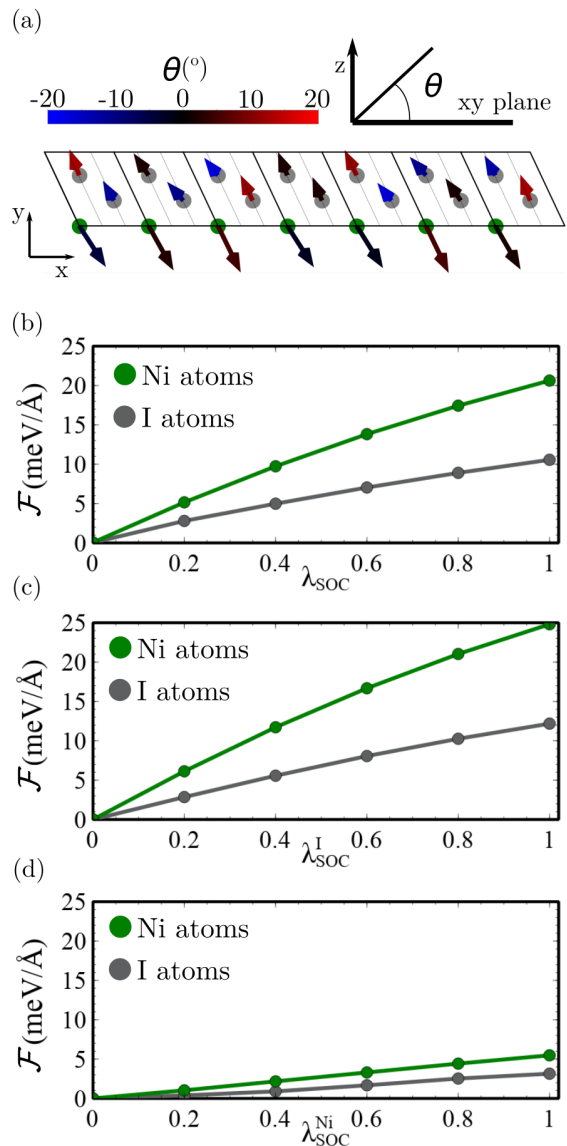


FIG. 4. (a) Real space plot of the ferroelectric force \mathcal{F}_α , highlighting the atomic relaxations associated to the emergence of a finite electric polarization. Panel (b) shows the scaling of the total ferroelectric force as a function of the SOC dimensionless parameter λ_{SOC} , highlighting the SOC origin of ferroelectric relaxations. Panel (c,d) show the ferroelectric force as a function of (c) the iodine SOC $\lambda_{\text{SOC}}^{\text{I}}$, taking $\lambda_{\text{SOC}}^{\text{Ni}} = 0$, and (d) as a function of the nickel SOC $\lambda_{\text{SOC}}^{\text{Ni}}$, taking $\lambda_{\text{SOC}}^{\text{I}} = 0$. This highlights the dominant role of iodine in generating the ferroelectric order and the opposite sign of the nickel contribution.

We show in Fig. 4a the ferroelectric force acting in the different iodine and Ni atoms. It is clearly observed that the ferroelectric polarization leads to an atomic displacement in the lattice. The previous results highlight that the combination of spin helical order and spin-orbit coupling leads not only to a ferroelectric order, but also to a strong magneto-elastic coupling.

We finally analyze the spin-orbit origin of the ferroelastic coupling. For this purpose, we now divide the den-

sity functional Hamiltonian into the relativistic and non-relativistic part as

$$\mathcal{H} = \mathcal{H}_0 + \lambda_{\text{SOC}} \mathcal{H}_{\text{SOC}} \quad (3)$$

where \mathcal{H}_0 is the non-relativistic Hamiltonian and \mathcal{H}_{SOC} is the relativistic spin-orbit coupling contribution. The parameter λ_{SOC} provides a knob to controllably switch on spin-orbit coupling, where $\lambda_{\text{SOC}} = 0$ corresponds to the non-relativistic calculations, and $\lambda_{\text{SOC}} = 1$ corresponds to the real spin-orbit coupling. We show in Fig. 4b the evolution of the average module of the ferroelectric force as a function of the spin-orbit parameter, computed for the two atomic species $\mathcal{F}_{\text{Ni}} = \langle |\mathcal{F}_\alpha| \rangle_{\text{Ni}}$ and $\mathcal{F}_{\text{I}} = \langle |\mathcal{F}_\alpha| \rangle_{\text{I}}$. In particular, it is clearly observed that the spiral-induced distortion of the lattice is zero in the absence of spin-orbit coupling, and it increases approximately linearly with the spin-orbit coupling, thus confirming the linear dependence with SOC anticipated for the $\xi \sim \lambda_{\text{SOC}}$ parameter in Eq. (1). This phenomenology shows that spin-orbit coupling is central in the induced ferroelastic coupling, in agreement with the electronic density reconstruction observed.

The previous ferroelectric force triggers a distortion of the lattice sites d on the order of 0.5pm, yielding a lattice contribution to the ferroelectric order. We can provide an estimate of the electric dipole in the monolayer p_{mono} associated to this distortion as $p_{\text{mono}} = dQ$, where $d = 0.5\text{pm}$ is the ferroelectric displacement and Q is the partial charge of the ions. We can estimate Q from our DFT calculations as the charge inside the muffin tin sphere of the Ni atoms, this corresponds to $Q = 0.9e$ with e the charge of the electron. We then obtain that $p_{\text{mono}} = 2 \cdot 10^{-2}$ D, this correspond to an electric polarization of the monolayer of $P_{\text{mono}} = 5 \cdot 10^{-13}$ C/m and $\xi \sim 10^{-21}$ C from eq. (1). As a reference, it is interesting to compare this value to the experimental one reported for bulk⁵². An experimental value for the volumetric electric polarization in bulk of $50 \cdot 10^{-6}$ C/m² is reported there. This leads to an electric polarization per layer of $P_{\text{bulk}} = 4 \cdot 10^{-14}$ C/m and an electric dipole per layer of $p_{\text{bulk}} = 10^{-3}$ D. Interestingly, the estimate we have obtained for the monolayer system overcomes the value reported for the bulk. Most importantly, this highlights that atomic displacements on the order $d = 0.5$ pm are not only sizable, but also would provide a ferroelectric order stronger than the bulk value. A more accurate determination of the electric polarization of the monolayer could be performed taking the full microscopic spatial dependence of the charge density, which would account for the partially covalent nature of NiI₂. Effectively, this would lead to a renormalization of the effective displaced charge q . Our estimate of the electric polarization of the monolayer is on the typical order of magnitude for spin-driven multiferroic mechanisms¹³.

To understand the contribution of the spin-orbit coupling of each element, we have further factored the full Hamiltonian in the form

$$\mathcal{H} = \mathcal{H}_0 + \lambda_{\text{SOC}}^{\text{Ni}} \mathcal{H}_{\text{SOC}}^{\text{Ni}} + \lambda_{\text{SOC}}^{\text{I}} \mathcal{H}_{\text{SOC}}^{\text{I}} \quad (4)$$

where $\lambda_{\text{SOC}}^{\text{Ni}}$, $\lambda_{\text{SOC}}^{\text{I}}$ controls the strength of the SOC in Ni and I, and $\mathcal{H}_{\text{SOC}}^{\text{Ni}}$, $\mathcal{H}_{\text{SOC}}^{\text{I}}$ are the two contributions to the spin-orbit coupling from Ni and I. To further demonstrate the dominating role of iodine, we switched off alternatively the SOC contribution of Ni ($\lambda_{\text{SOC}}^{\text{Ni}} = 0$ in Fig. 4c) and I ($\lambda_{\text{SOC}}^{\text{I}} = 0$ in Fig. 4d) and computed the ferroelectric force as a function of the other one $\lambda_{\text{SOC}}^{\text{I, Ni}}$, respectively. In particular, as shown in Fig. 4c, we observe that the ferroelectric force yields nearly identical values to the calculations with full SOC, demonstrating that the dominant contribution to the ferroelectric force arises from the iodine spin-orbit coupling. In stark contrast, if only the spin-orbit contribution of Ni is included, the ferroelectric force would become much smaller as shown in Fig. 4d. Indeed, comparing Figs. 4b and 4c, it can be observed that the SOC contribution from the Ni atoms acts in the opposite way to the I contribution for the emergence of a ferroelectric polarization. The previous phenomenology stems from the fact that SOC of I atoms is one order of magnitude higher than that of Ni atoms, leading to iodine spin-orbit coupling as the dominating contribution to the 2D multiferroic order in NiI₂.

Finally, we comment on the implications of the previous phenomenology. First, the ferroelectric polarization is uniquely determined by the spiral \mathbf{q} -vector. This implies that in a magnetic domain wall between different \mathbf{q} -vectors will lead to an associated domain wall between in the ferroelectric polarizations⁵³. Second, the magnetic origin of the ferroelectric polarization accounts for the development of ferroelectric polarization right at the magnetic ordering temperatures as observed experimentally²⁷. Therefore, the melting of multiferroicity will be associated to the thermal quench of magnetic order. For a 2D magnetic monolayer with magnetic anisotropy, the melting of magnetic ordering is associated to the thermal excitation of magnetic fluctuations^{25,48,49,54}. These lead to a critical point at an energy scale controlled by the exchange coupling and the magnetic anisotropy^{48,55}. As the parent magnetic ordering is quenched with increasing temperature, so is the ferroelectric ordering, leading to leading to a simultaneous melting of the two orders associated to the multiferroic behavior^{12,13}. Moreover, the energy to flip the ferroelectric polarization will be given by the magnetic exchange, since switching the ferroelectric domain requires switching the magnetic one¹³. However, we have to note that, besides these energetic considerations, the required voltage to create the transition will also depend on the magnetoelectric path followed by the system and the electronic screening of the device. Importantly, the crucial role of spin-orbit coupling observed in Fig. 4 suggests that ferroelastic couplings can be tunable by means of spin-orbit engineering^{56,57}. The strong locking of ferroelectric and magnetic order highlights that conventional strategies of tuning magnetic ordering such as gating¹⁵,

strain^{58–60} and exchange proximity²² can have a dramatic impact on the ferroelectric polarization of the monolayer. As a consequence, the strong magneto-elastic coupling suggests that twisted multilayers of NiI₂ can potentially show emergent moire spiral and ferroelectric orders due to the stacking-induced modulations of the interlayer exchange coupling^{61,62}.

V. CONCLUSIONS

We have shown that the multiferroic behavior in monolayer NiI₂ stems from the interplay of spin helical order and spin-orbit coupling. In particular, using first-principles calculations, the strong spin-orbit coupling of iodine was shown to dominate the electronic reconstruction leading to the in-plane ferroelectric order. Interestingly, the strongest charge reconstruction leading to the ferroelectric order emerges around the iodine atoms, which is accompanied by a sizable local magnetization in iodine. This highlights the fine interplay between spin-orbit coupling and spin non-collinearity as driving forces for multiferroic order, leading to a locking between mag-

netic helical and ferroelectric orders. Furthermore, associated with the electronic ferroelectric order, a structural distortion is triggered in the lattice leading to strong magneto-elastic coupling in monolayer NiI₂. Our results show the relativistic origin of multiferroic order in monolayer NiI₂, providing a microscopic mechanism accounting for the simultaneous ferroelectric and magnetic ordering. These results provide a starting point towards controlling multiferroicity in monolayer NiI₂ by means of gating, chemical engineering, twist engineering, and proximity effects, ultimately leading to a new family of designer van der Waals multiferroics.

ACKNOWLEDGEMENTS

We acknowledge the computational resources provided by the Aalto Science-IT project, and the financial support from the Academy of Finland Projects No. 331342 and No. 336243, and the Jane and Aatos Erkkö Foundation. We thank P. Liljeroth, S. Kezilebieke and V. Pardo for useful discussions.

-
- ¹ A. K. Geim and I. V. Grigorieva, “Van der waals heterostructures,” *Nature* **499**, 419–425 (2013).
 - ² Miguel M. Ugeda, Aaron J. Bradley, Yi Zhang, Seita Onishi, Yi Chen, Wei Ruan, Claudia Ojeda-Aristizabal, Hyejin Ryu, Mark T. Edmonds, Hsin-Zon Tsai, and et al., “Characterization of collective ground states in single-layer nbse2,” *Nature Physics* **12**, 92–97 (2015).
 - ³ Sergio C. de la Barrera, Michael R. Sinko, Devashish P. Gopalan, Nikhil Sivadas, Kyle L. Seyler, Kenji Watanabe, Takashi Taniguchi, Adam W. Tsen, Xiaodong Xu, Di Xiao, and et al., “Tuning ising superconductivity with layer and spin-orbit coupling in two-dimensional transition-metal dichalcogenides,” *Nature Communications* **9** (2018), 10.1038/s41467-018-03888-4.
 - ⁴ Zaiyao Fei, Bevin Huang, Paul Malinowski, Wenbo Wang, Tiancheng Song, Joshua Sanchez, Wang Yao, Di Xiao, Xiaoyang Zhu, Andrew F. May, Weida Wu, David H. Cobden, Jiun-Haw Chu, and Xiaodong Xu, “Two-dimensional itinerant ferromagnetism in atomically thin fe3gete2,” *Nature Materials* **17**, 778–782 (2018).
 - ⁵ Bevin Huang, Genevieve Clark, Efrén Navarro-Moratalla, Dahlia R. Klein, Ran Cheng, Kyle L. Seyler, Ding Zhong, Emma Schmidgall, Michael A. McGuire, David H. Cobden, Wang Yao, Di Xiao, Pablo Jarillo-Herrero, and Xiaodong Xu, “Layer-dependent ferromagnetism in a van der waals crystal down to the monolayer limit,” *Nature* **546**, 270–273 (2017).
 - ⁶ Jae-Ung Lee, Sungmin Lee, Ji Hoon Ryoo, Soonmin Kang, Tae Yun Kim, Pilkwang Kim, Cheol-Hwan Park, Je-Geun Park, and Hyeonsik Cheong, “Ising-type magnetic ordering in atomically thin feps3,” *Nano Letters* **16**, 7433–7438 (2016).
 - ⁷ Cheng Gong, Lin Li, Zhenglu Li, Huiwen Ji, Alex Stern, Yang Xia, Ting Cao, Wei Bao, Chenzhe Wang, Yuan Wang, Z. Q. Qiu, R. J. Cava, Steven G. Louie, Jing Xia, and Xiang Zhang, “Discovery of intrinsic ferromagnetism in two-dimensional van der waals crystals,” *Nature* **546**, 265–269 (2017).
 - ⁸ Zhaowei Zhang, Jingzhi Shang, Chongyun Jiang, Abdullah Rasmita, Weibo Gao, and Ting Yu, “Direct photoluminescence probing of ferromagnetism in monolayer two-dimensional crbr3,” *Nano Letters* **19**, 3138–3142 (2019).
 - ⁹ Chaojie Cui, Wei-Jin Hu, Xingxu Yan, Christopher Addiego, Wenpei Gao, Yao Wang, Zhe Wang, Linze Li, Yingchun Cheng, Peng Li, Xixiang Zhang, Husam N. Alshareef, Tom Wu, Wenguang Zhu, Xiaoqing Pan, and Lain-Jong Li, “Intercorrelated in-plane and out-of-plane ferroelectricity in ultrathin two-dimensional layered semiconductor in2se3,” *Nano Letters* **18**, 1253–1258 (2018).
 - ¹⁰ Shuoguo Yuan, Xin Luo, Hung Lit Chan, Chengcheng Xiao, Yawei Dai, Maohai Xie, and Jianhua Hao, “Room-temperature ferroelectricity in mote2 down to the atomic monolayer limit,” *Nature Communications* **10**, 1775 (2019).
 - ¹¹ Nicola A. Hill, “Why are there so few magnetic ferroelectrics?” *The Journal of Physical Chemistry B* **104**, 6694–6709 (2000).
 - ¹² R. RAMESH and NICOLA A. SPALDIN, “Multiferroics: progress and prospects in thin films,” *Nanoscience and Technology*, 20–28 (2009).
 - ¹³ Manfred Fiebig, Thomas Lottermoser, Dennis Meier, and Morgan Trassin, “The evolution of multiferroics,” *Nature Reviews Materials* **1** (2016), 10.1038/natrevmats.2016.46.
 - ¹⁴ Yujun Deng, Yijun Yu, Yichen Song, Jingzhao Zhang, Nai Zhou Wang, Zeyuan Sun, Yangfan Yi, Yi Zheng Wu, Shiwei Wu, Junyi Zhu, and et al., “Gate-tunable room-temperature ferromagnetism in two-dimensional fe3gete2,” *Nature* **563**, 94–99 (2018).

- ¹⁵ Bevin Huang, Genevieve Clark, Dahlia R. Klein, David MacNeill, Efrén Navarro-Moratalla, Kyle L. Seyler, Nathan Wilson, Michael A. McGuire, David H. Cobden, Di Xiao, and et al., “Electrical control of 2d magnetism in bilayer cri3,” *Nature Nanotechnology* **13**, 544–548 (2018).
- ¹⁶ M. Gibertini, M. Koperski, A. F. Morpurgo, and K. S. Novoselov, “Magnetic 2d materials and heterostructures,” *Nature Nanotechnology* **14**, 408–419 (2019).
- ¹⁷ D. R. Klein, D. MacNeill, J. L. Lado, D. Soriano, E. Navarro-Moratalla, K. Watanabe, T. Taniguchi, S. Manni, P. Canfield, J. Fernández-Rossier, and et al., “Probing magnetism in 2d van der waals crystalline insulators via electron tunneling,” *Science* **360**, 1218–1222 (2018).
- ¹⁸ Shawulien Kezilebieke, Md Nurul Huda, Paul Dreher, Ilkka Manninen, Yifan Zhou, Jani Sainio, Rhodri Mansell, Miguel M. Ugeda, Sebastiaan van Dijken, Hannu-Pekka Komsa, and et al., “Electronic and magnetic characterization of epitaxial vse2 monolayers on superconducting nbse2,” *Communications Physics* **3** (2020), 10.1038/s42005-020-0377-4.
- ¹⁹ Kyle L. Seyler, Ding Zhong, Bevin Huang, Xiayu Linpeng, Nathan P. Wilson, Takashi Taniguchi, Kenji Watanabe, Wang Yao, Di Xiao, Michael A. McGuire, and et al., “Valley manipulation by optically tuning the magnetic proximity effect in wse2/cr3 heterostructures,” *Nano Letters* **18**, 3823–3828 (2018).
- ²⁰ Yurong Su, Xinlu Li, Meng Zhu, Jia Zhang, Long You, and Evgeny Y. Tsymlal, “Van der waals multiferroic tunnel junctions,” *Nano Letters* **21**, 175–181 (2020).
- ²¹ Viliam Vaño, Mohammad Amini, Somesh Chandra Ganguli, Guangze Chen, Jose L. Lado, Shawulien Kezilebieke, and Peter Liljeroth, “Artificial heavy fermions in a van der Waals heterostructure,” arXiv e-prints, arXiv:2103.11989 (2021), arXiv:2103.11989 [cond-mat.mes-hall].
- ²² Chuan Zhao, Tenzin Norden, Peiyao Zhang, Puqin Zhao, Yingchun Cheng, Fan Sun, James P. Parry, Payam Taheri, Jieqiong Wang, Yihang Yang, and et al., “Enhanced valley splitting in monolayer wse2 due to magnetic exchange field,” *Nature Nanotechnology* **12**, 757–762 (2017).
- ²³ Shawulien Kezilebieke, Md Nurul Huda, Viliam Vaño, Markus Aapro, Somesh C. Ganguli, Orlando J. Silveira, Szczepan Głodzik, Adam S. Foster, Teemu Ojanen, and Peter Liljeroth, “Topological superconductivity in a van der waals heterostructure,” *Nature* **588**, 424–428 (2020).
- ²⁴ Michael McGuire, “Crystal and magnetic structures in layered, transition metal dihalides and trihalides,” *Crystals* **7**, 121 (2017).
- ²⁵ M. Blei, J. L. Lado, Q. Song, D. Dey, O. Erten, V. Pardo, R. Comin, S. Tongay, and A. S. Botana, “Synthesis, engineering, and theory of 2d van der waals magnets,” *Applied Physics Reviews* **8**, 021301 (2021).
- ²⁶ Hwiin Ju, Youjin Lee, Kwang-Tak Kim, In Hyeok Choi, Chang Jae Roh, Suhan Son, Pyeongjae Park, Jae Ha Kim, Taek Sun Jung, Jae Hoon Kim, and et al., “Possible persistence of multiferroic order down to bilayer limit of van der waals material nii2,” *Nano Letters* **21**, 5126–5132 (2021).
- ²⁷ Qian Song, Connor A. Occhialini, Emre Ergeçen, Batyr Ilyas, Kenji Watanabe, Takashi Taniguchi, Nuh Gedik, and Riccardo Comin, “Experimental realization of a single-layer multiferroic,” arXiv e-prints, arXiv:2106.07661 (2021), arXiv:2106.07661 [cond-mat.str-el].
- ²⁸ Maxim Mostovoy, “Ferroelectricity in spiral magnets,” *Phys. Rev. Lett.* **96**, 067601 (2006).
- ²⁹ Hosho Katsura, Naoto Nagaosa, and Alexander V. Balatsky, “Spin current and magnetoelectric effect in non-collinear magnets,” *Phys. Rev. Lett.* **95**, 057205 (2005).
- ³⁰ Chenglong Jia, Shigeki Onoda, Naoto Nagaosa, and Jung Hoon Han, “Bond electronic polarization induced by spin,” *Phys. Rev. B* **74**, 224444 (2006).
- ³¹ P. Hohenberg and W. Kohn, “Inhomogeneous electron gas,” *Phys. Rev.* **136**, B864–B871 (1964).
- ³² “Elk code,” <http://elk.sourceforge.net/>.
- ³³ W. Kohn and L. J. Sham, “Self-consistent equations including exchange and correlation effects,” *Phys. Rev.* **140**, A1133–A1138 (1965).
- ³⁴ S.R. Kuindersma, J.P. Sanchez, and C. Haas, “Magnetic and structural investigations on nii2 and coi2,” *Physica B+C* **111**, 231–248 (1981).
- ³⁵ D. Billerey, C. Terrier, N. Ciret, and J. Kleinclauss, “Neutron diffraction study and specific heat of antiferromagnetic nii2,” *Physics Letters A* **61**, 138–140 (1977).
- ³⁶ The vector of the bulk helimagnetic state is $\mathbf{q} = 0.138\mathbf{b}_1 + 1.457\mathbf{b}_3$, where \mathbf{b}_1 , \mathbf{b}_3 are the reciprocal lattice vectors.
- ³⁷ We neglect the out-of-plane component of the spin propagation as we are in the monolayer limit and it is one order of magnitude smaller than the in-plane component.
- ³⁸ Due to a d-d character of the energy gap, electronic correlations are expected to increase the value predicted by LDA, thus approaching the experimental value reported for the bulk⁶³.
- ³⁹ P. W. Anderson, “Antiferromagnetism. theory of superexchange interaction,” *Phys. Rev.* **79**, 350–356 (1950).
- ⁴⁰ John B. Goodenough, “An interpretation of the magnetic properties of the perovskite-type mixed crystals $\text{La}_1-x\text{Sr}_x\text{CoO}_3$,” **6**, 287–297 (1958).
- ⁴¹ Junjiro Kanamori, “Superexchange interaction and symmetry properties of electron orbitals,” *Journal of Physics and Chemistry of Solids* **10**, 87–98 (1959).
- ⁴² Michael McGuire, “Crystal and magnetic structures in layered, transition metal dihalides and trihalides,” *Crystals* **7**, 121 (2017).
- ⁴³ I. Dzyaloshinsky, “A thermodynamic theory of “weak” ferromagnetism of antiferromagnetics,” *Journal of Physics and Chemistry of Solids* **4**, 241–255 (1958).
- ⁴⁴ Danila Amoroso, Paolo Barone, and Silvia Picozzi, “Spontaneous skyrmionic lattice from anisotropic symmetric exchange in a ni-halide monolayer,” *Nature Communications* **11**, 5784 (2020).
- ⁴⁵ Tôru Moriya, “Anisotropic superexchange interaction and weak ferromagnetism,” *Phys. Rev.* **120**, 91–98 (1960).
- ⁴⁶ P. C. Hohenberg, “Existence of long-range order in one and two dimensions,” *Phys. Rev.* **158**, 383–386 (1967).
- ⁴⁷ N. D. Mermin and H. Wagner, “Absence of ferromagnetism or antiferromagnetism in one- or two-dimensional isotropic heisenberg models,” *Phys. Rev. Lett.* **17**, 1133–1136 (1966).
- ⁴⁸ J L Lado and J Fernández-Rossier, “On the origin of magnetic anisotropy in two dimensional cri 3,” *2D Materials* **4**, 035002 (2017).
- ⁴⁹ D. Soriano, M. I. Katsnelson, and J. Fernández-Rossier, “Magnetic two-dimensional chromium trihalides: A theoretical perspective,” *Nano Letters* **20**, 6225–6234 (2020).
- ⁵⁰ P.C. Hohenberg and A.P. Krekhov, “An introduction to the ginzburg–landau theory of phase transitions and nonequilibrium patterns,” *Physics Reports* **572**, 1–42 (2015).
- ⁵¹ We take as initial structure the fully relaxed structure in the minimal unit cell.

- ⁵² T. Kurumaji, S. Seki, S. Ishiwata, H. Murakawa, Y. Kaneko, and Y. Tokura, “Magnetoelectric responses induced by domain rearrangement and spin structural change in triangular-lattice helimagnets NiI_2 and CoI_2 ,” *Phys. Rev. B* **87**, 014429 (2013).
- ⁵³ J. Seidel, L. W. Martin, Q. He, Q. Zhan, Y.-H. Chu, A. Rother, M. E. Hawkrigde, P. Maksymovych, P. Yu, M. Gajek, and et al., “Conduction at domain walls in oxide multiferroics,” *Nature Materials* **8**, 229–234 (2009).
- ⁵⁴ Kenneth S. Burch, David Mandrus, and Je-Geun Park, “Magnetism in two-dimensional van der waals materials,” *Nature* **563**, 47–52 (2018).
- ⁵⁵ Daniele Torelli and Thomas Olsen, “Calculating critical temperatures for ferromagnetic order in two-dimensional materials,” *2D Materials* **6**, 015028 (2018).
- ⁵⁶ Mykola Abramchuk, Samantha Jaszewski, Kenneth R. Metz, Gavin B. Osterhoudt, Yiping Wang, Kenneth S. Burch, and Fazel Tafti, “Controlling magnetic and optical properties of the van der waals crystal CrCl_3Br_x via mixed halide chemistry,” *Advanced Materials* **30**, 1801325 (2018).
- ⁵⁷ Thomas A. Tartaglia, Joseph N. Tang, Jose L. Lado, Faranak Bahrami, Mykola Abramchuk, Gregory T. McCandless, Meaghan C. Doyle, Kenneth S. Burch, Ying Ran, Julia Y. Chan, and et al., “Accessing new magnetic regimes by tuning the ligand spin-orbit coupling in van der waals magnets,” *Science Advances* **6** (2020), 10.1126/sciadv.abb9379.
- ⁵⁸ Lucas Webster and Jia-An Yan, “Strain-tunable magnetic anisotropy in monolayer CrCl_3 , CrBr_3 , and CrI_3 ,” *Phys. Rev. B* **98**, 144411 (2018).
- ⁵⁹ Adolfo O. Fumega, M. Gobbi, P. Dreher, W. Wan, C. González-Orellana, M. Peña-Díaz, C. Rogero, J. Herrero-Martín, P. Gargiani, M. Ilyn, and et al., “Absence of ferromagnetism in VSe_2 caused by its charge density wave phase,” *The Journal of Physical Chemistry C* **123**, 27802–27810 (2019).
- ⁶⁰ Adolfo Otero Fumega, Jan Phillips, and Victor Pardo, “Controlled two-dimensional ferromagnetism in 1t-CrTe_2 : The role of charge density wave and strain,” *The Journal of Physical Chemistry C* **124**, 21047–21053 (2020).
- ⁶¹ Nikhil Sivadas, Satoshi Okamoto, Xiaodong Xu, Craig J. Fennie, and Di Xiao, “Stacking-dependent magnetism in bilayer CrI_3 ,” *Nano Letters* **18**, 7658–7664 (2018).
- ⁶² D. Soriano, C. Cardoso, and J. Fernández-Rossier, “Interplay between interlayer exchange and stacking in CrI_3 bilayers,” *Solid State Communications* **299**, 113662 (2019).
- ⁶³ C. R. Ronda, G. J. Arends, and C. Haas, “Photoconductivity of the nickel dihalides and the nature of the energy gap,” *Phys. Rev. B* **35**, 4038–4043 (1987).